Effect of BBSZ-LMZBS Co-doped NiCuZn Ferrite on Gyromagnetic, Soft and Static Magnetic Properties

Qingmei Xu*

Department of Electrical Engineering, Taiyuan Institute of Technology, Taiyuan 030008, China

(Received 23 January 2025, Received in final form 22 July 2025, Accepted 25 July 2025)

In this study, BBSZ-LMZBS co-doped $Ni_{0.22}Cu_{0.31}Zn_{0.47}Fe_2O_4$ -based ferrites were prepared by low temperature (880 °C) solid state reaction. The microstructure, static magnetic, soft magnetic and gyromagnetic properties of NiCuZn ferrites with different doping amounts were studied. XRD and SEM showed that the samples were successfully synthesized, and BBSZ-LMZBS promoted the low-temperature sintering of the samples through the liquid phase sintering mechanism. With the increase of the doping amount of BBSZ-LMZBS, the static magnetic property M_s of the sample reaches a maximum value of 94.42 emu/g (x=0.35), and H_c reaches a minimum value of 81.84 Oe (x=0.40). From x=0.05 to 0.40, the soft magnetic property μ' value of the sample decreases by 40% (from 30.6 to 9.3), the ε' value decreases from 21.8 to about 13, and the tan δ value remains small and stable. The gyromagnetic property value of the sample at 9.55GHz decreases from 872 Oe to 230 Oe, a decrease of 24%.

Keywords: NiCuZn ferrites, gyromagnetic properties, soft magnetic, static magnetic

1. Introduction

In recent years, with the development of 5G communication technology and the continuous exploration of future 6G technology, more stringent requirements have been placed on electronic components, such as miniaturization, integration, and multi-functions [1, 2]. Therefore, exploring a multifunctional and excellent performance material to achieve good matching and high-density integration of different devices will be more conducive to the application of 5G and the exploration of 6G [3]. Ferrite materials have always attracted the attention of many researchers due to their excellent soft magnetic, gyromagnetic and dielectric properties [4, 5]. NiCuZn ferrite, an important part of ferrite, is widely used in the field of electronic communications due to its excellent properties such as high resistivity, high density, medium dielectric constant and low dielectric loss. For example, micro-sensors, complex LTCC multilayer devices, EMI filters, radio identification communications and multilayer chip inductors, etc [6]. Low temperature co-fired ceramics (LTCC) is one of the key technologies for device integration. It can be used in 3D stacked electronic components and has received worldwide attention. Therefore, low temperature sintering of NiCuZn ferrite and continuously improving its electromagnetic properties has become an important research topic [7].

In previous studies, researchers often added oxides with lower melting points or changed the element ratio of NiCuZn to reduce the sintering temperature. Wang et al. studied the effect of Sb₂O₃-doped on the cutoff frequency of NiCuZn sintered in LTCC [8]. Zhang et al. added Bi₂O₃-Co₂O₃ to lower the sintering temperature and analyzed its effect on the microstructure and electromagnetic properties [9]. It is reported that BBSZ (Bi₂O₃-H₃BO₃-SiO₂-ZnO) is a good sintering temperature controller, while LMZBS (Li₂CO₃-MgO-ZnO-B₂O₃-SiO₂) is a good additive for LiZn ferrite to reduce the sintering temperature [4, 10]. The effect of co-addition of BBSZ and LMZBS on the properties of NiCuZn ferrite has not been reported.

In this paper, we used a solid phase reaction method and low temperature sintering to modify Ni_{0.22}Cu_{0.31}Zn_{0.47}Fe₂O₄ samples. BBSZ and variable amounts of LMZBS were added to the samples, and the microstructure, static magnetic properties, soft magnetic properties and gyromagnetic properties in the millimeter wave band were systematically studied. It is worth noting that by adding BBSZ and LMZBS to solve the common problems of insufficient grain growth during low-temperature sintering, high porosity and poor

©The Korean Magnetics Society. All rights reserved. *Corresponding author: Tel: +86-13303517119

e-mail: qmxu@stu.pku.edu.cn

density, a NiCuZn ferrite sample with excellent gyromagnetic properties was finally prepared. The samples can be used to prepare 3D integrated devices for 5G/6G/millimeter wave band through LTCC technology [5].

2. Experimental

2.1. Sample preparation

First, we synthesize the co-solvent BBSZ/LMZBS. BBSZ was synthesized with a molar ratio of 27% Bi₂O₃-35% H₃BO₃-6% SiO₂-32% ZnO. The raw materials were weighed, ground, mixed, and then the mixture was heated to 1000 °C for 1 h. LMZBS was synthesized with a molar ratio of 25% Li₂O-25% MgO-25% ZnO-25% B₂O₃-25% SiO₂. The raw materials were weighed, ground, mixed, and then the mixture was heated to 1400 °C for 1 h. After heating, the BBSZ/LMZBS powder was rapidly quenched in deionized water and finally uniformly ground with an agate, respectively. Finally, the BBSZ/LMZBS co-solvent body was obtained.

NiCuZn ferrite samples with the composition Ni_{0.22}Cu_{0.31}Zn_{0.47}Fe₂O₄ were prepared by the conventional mixed-oxide method. First, appropriate amounts of highpurity NiO, CuO, ZnO and Fe₃O₄ powders were weighed and wet-mixed in a ball mill. Deionized water was added to the powders, and the powders were mixed in a ball mill with nylon balls (the balls were 10 mm or 6 mm in diameter) at a running speed of 220 rpm for 24 h. Next, these powders were dried and calcined at 880 °C for 2 h in air to prepare spinel-type ferrite powders. Then, 0.1 wt% BBSZ and x wt% LMZBS (x=0.05, 0.10, 0.15, 0.20, 0.25, 0.30, 0.35, 0.40) were added into calcined powders as sintering aid and milled again for 24 h. These mixtures were pressed into toroidal samples with 10 wt% of PVA binder under a pressure of 20 MPa. Finally, the samples were sintered in atmospheric pressure at 880 °C.

2.2. Testing and characterization

The phase compositions of the samples were characterized by X-ray diffraction (XRD) (D/max 2400, Rigaku, Tokyo Japan) using Cu- $K\alpha$ radiation. The diffraction patterns were measured over a scanning angle range from 10° to 70° with a step width of 0.02°. The microstructures were imaged with scanning electron microscopy (SEM) (JSM 6490LV, JEOL, Tokyo Japan). The soft magnetic properties were measured using an Hp-4291B RF Impedance Analyzer. Magnetization hysteresis loops were measured with applied field up to 5000 Oe using a vibrating sample magnetometer (BHV-525, Riken Denshi, Tokyo Japan). The ferromagnetic resonance (FMR) linewidth of the samples was measured in a TE106 transmission resonant cavity. The ΔH was

measured in TE106 perturbation method cavity at 9.55 GHz (the sample was ground into a single sphere with diameter of about 0.6 mm).

3. Results and Discussion

3.1. Phase and microstructure

Fig. 1 shows the XRD patterns measured for Ni_{0.22}Cu_{0.31}Zn_{0.47}Fe₂O₄ ferrite doped with 0.1 wt% BBSZ and x wt% LMZBS (x=0.05~0.40). All the XRD peaks were indexed to the standard PDF card JCPDS-51-0386. Typical diffraction peaks of the NiCuZn spinel structure are marked as (220), (311), (400), (511) and (440). No diffraction peaks of other crystalline phases were observed in the figure, so all samples were successfully synthesized. From Fig. 1, as the doping amount of BBSZ-LMZBS increases, the intensity of its diffraction peaks (511) and (440) increases. It shows that the doping of BBSZ-LMZBS helps the sample to sinter at low temperature. When the doping amount is small, the grains fail to grow fully, resulting in a low diffraction peak intensity. When the doping amount is large, the sample has sufficient grain growth at 880 °C and good crystallinity [11, 12]. This phenomenon occurs due to the doping of BBSZ-LMZBS reduces the sintering temperature of NiCuZn and promotes the growth of grains.

Fig. 2 shows the cross-sectional SEM images of the samples at magnification of ×5000x. As can be seen from Fig. 2, the sample was sintered at a low temperature of 880 °C, and its crystal phase was small. In addition, due to the addition of amorphous BBSZ-LMZBS, the grain boundaries are unclear, and the grains are bonded together.

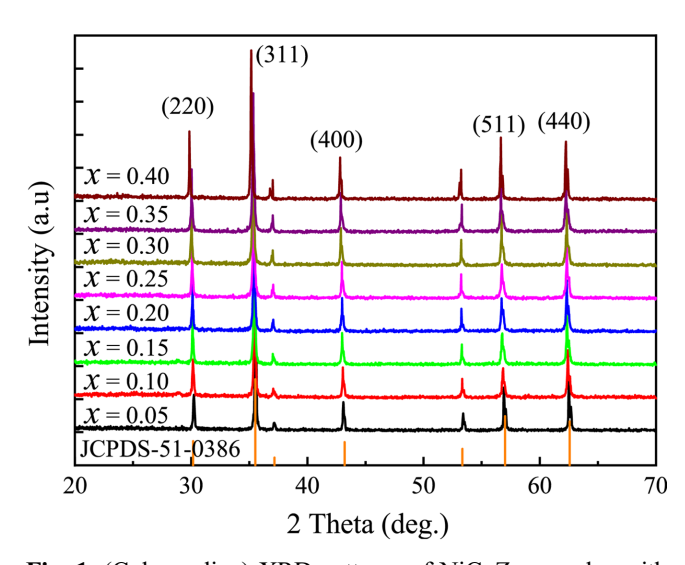


Fig. 1. (Color online) XRD patterns of NiCuZn samples with different x contents of BBSZ-LMZBS.

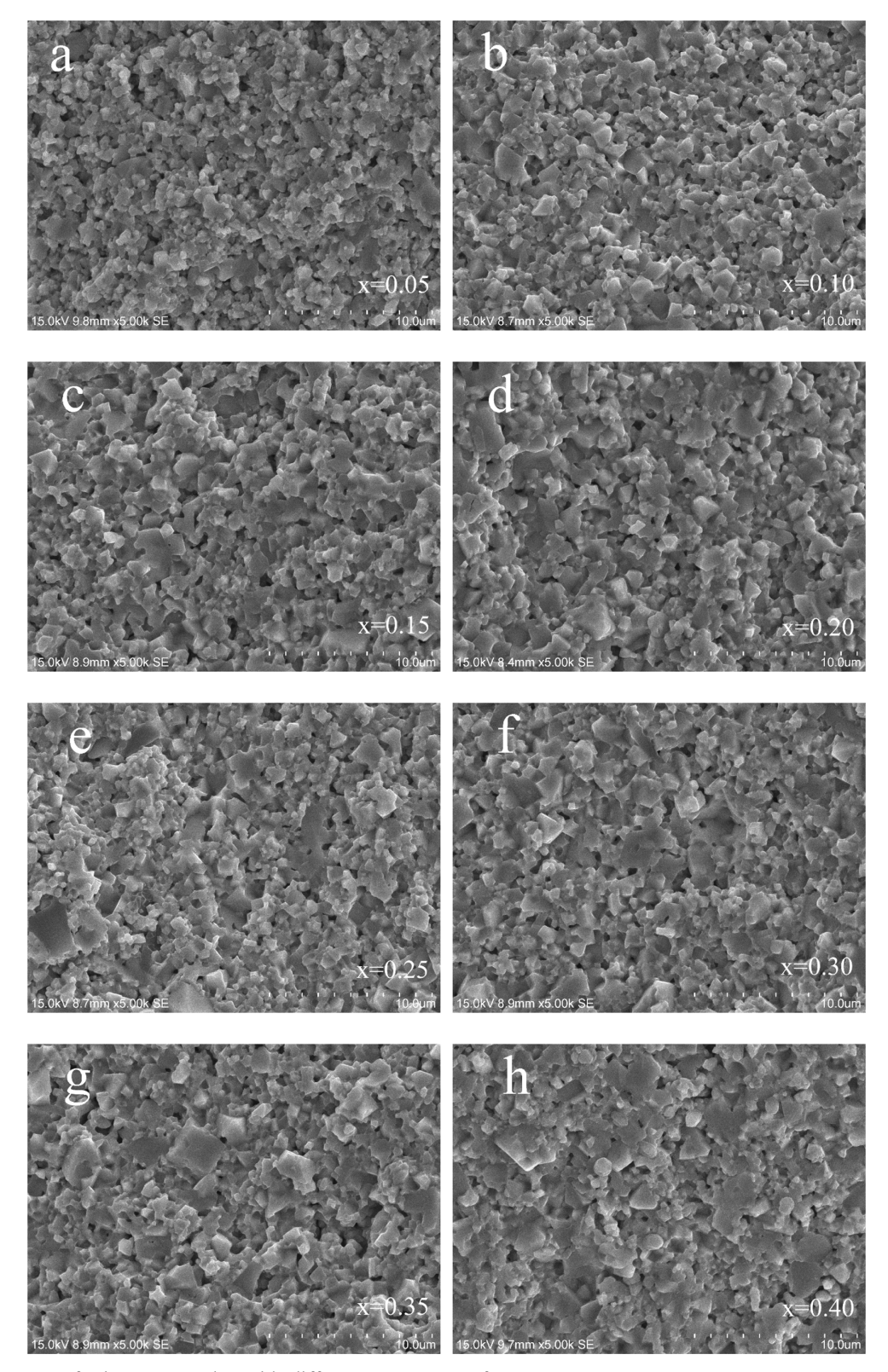


Fig. 2. SEM images of NiCuZn samples with different x contents of BBSZ-LMZBS.

Fig. 2a shows that the grains are small and uniform in size, with basically no large grains, and Fig. 2h shows the appearance of more large grains. The changes in the

sample microstructure show that with the increase in the doping amount of BBSZ-LMZBS, on the one hand, several small grains gradually bond together to form larger grains, and

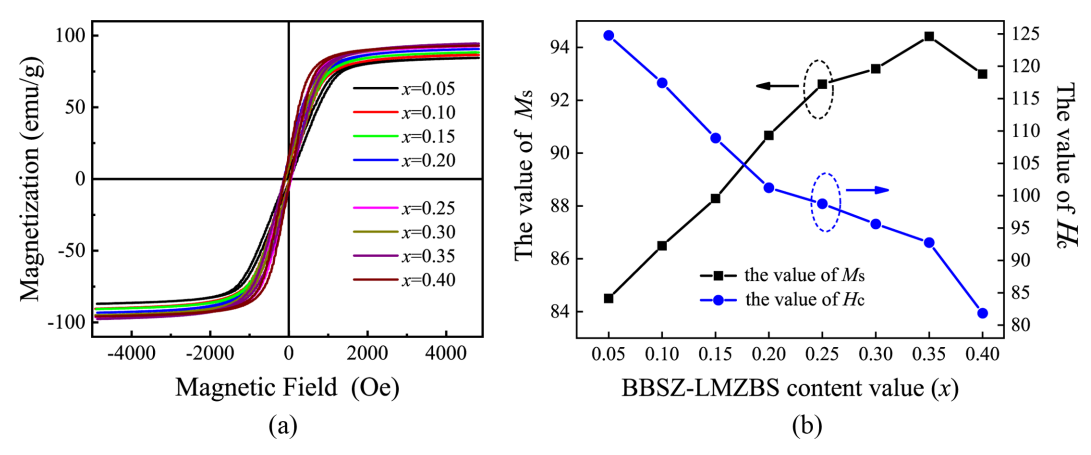


Fig. 3. (Color online) The magnetic properties of the BBSZ-LMZBS doped samples. (a) M-H curves measured up to 5.0 KOe, (b) The curve of M_s and H_c with different x contents of BBSZ-LMZBS.

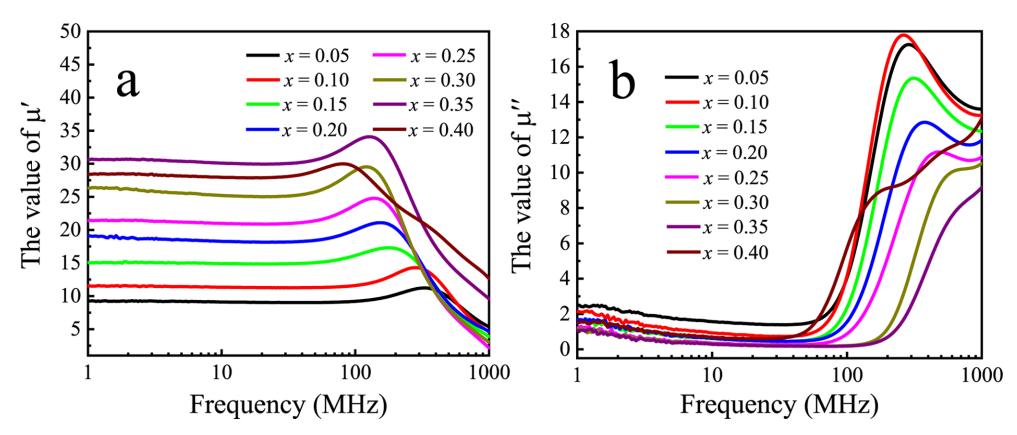


Fig. 4. (Color online) The complex permeability (μ' and μ'') of the BBSZ-LMZBS doped samples at 1 MHz-1 GHz as a function of frequency.

on the other hand, BBSZ-LMZBS as a non-crystalline substance fills the gaps between the grains. The cross-sectional SEM photo confirms that BBSZ-LMZBS promotes the low-temperature sintering of the sample through the liquid phase sintering mechanism. As a glassy substance, BBSZ-LMZBS forms a liquid phase during the sintering process, which can greatly reduce the sintering activation energy of NiCuZn and improve the low-temperature sintering characteristics of the sample.

3.2. Static magnetic performance

Fig. 3a shows the magnetic hysteresis loops of NiCuZn ferrites. Fig. 3b presents the values of saturation magnetization (M_s) and intrinsic coercivity (H_c) obtained from the Fig. 3a. shows that the value of M_s first increased and then decreased, as the amount of BBSZ-LMZBS addition increases from 0.05 to 0.40. the maximum value of M_s can reach 94.42 emu/g when x=0.35. The M_s is 84.5 emu/g, 86.49 emu/g, 88.28 emu/g, 90.67 emu/g, 92.64 emu/g, 93.19 emu/g, 94.42 emu/g, 92.99 emu/g from x=0.20 to 0.40, respectively.

The main factors affecting the M_s include grain size, lattice, and the distribution of metal elements in the crystal structure [8, 13]. From the XRD results, the lattice constant of the samples prepared by different contents of BBSZ-LMZBS does not change much, but it has a certain effect on the grain size. The average grain size of the sample with content x=0.40 is the largest, but the M_s corresponding to the sample with content x=0.35 is the largest, which may be due to the excessive additives that deteriorate the static magnetic properties of the sample. However, the H_c presents the monotone decreasing tendency. The H_c is 124.77 Oe, 117.45 Oe, 108.91 Oe, 101.24 Oe, 98.75 Oe, 95.64 Oe, 92.77 Oe, 81.84 Oe, from x=0.20 to 0.40, respectively. One reason is that its grain size is large and grain boundary is thin, on the other hand, its crystal structure is complete and its internal stress is small [14].

3.3. Soft magnetic performance

Fig. 4 shows the real and imaginary parts of relative complex permeability. Fig. 4a is the real part of the measured

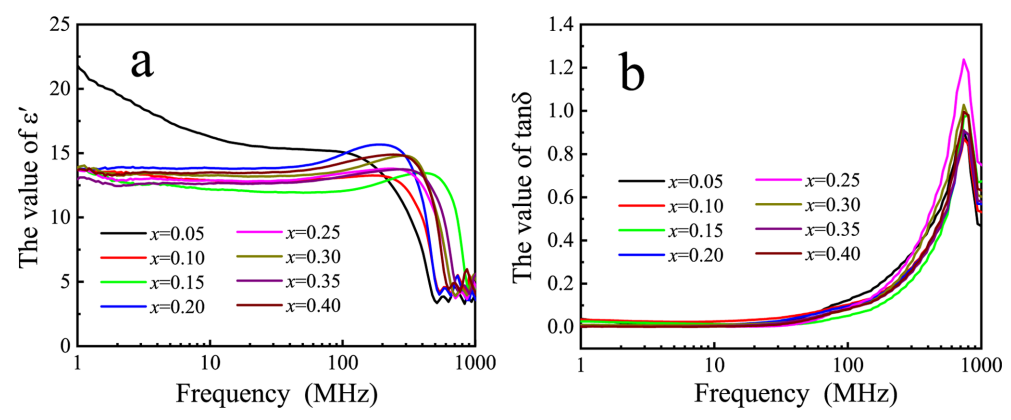


Fig. 5. (Color online) The complex permittivity (ϵ' and $\tan\delta$) of the BBSZ-LMZBS doped samples as a function of frequency from 1 MHz to 1 GHz.

magnetic permeability (μ') , and Fig. 4b is the imaginary part of the measured magnetic permeability (μ''). The μ' represents the material's ability to respond to a magnetic field, whereas the μ'' represents magnetic losses within the material. The μ' maintains a stable value in the range of 1 MHz-100 MHz, and the μ'' also remains around 1.1-2.4 in this frequency range. The value of μ' at 1MHz are 9.3, 11.5, 15.0, 19.1, 21.4, 26.3, 30.6 and 28.4, for x=0.05~0.40, respectively. As the BBSZ-LMZBS content increased, the μ' increased and then decreased, indicating that the BBSZ-LMZBS addition changed soft magnetic performance. When the BBSZ-LMZBS content x=0.35, the μ' reaches a maximum value of 30.6, and then decreases. The BBSZ-LMZBS content helps to control the initial magnetic permeability of the NiCuZn sample. It is well known that the change in permeability is caused by two types of magnetization mechanisms, namely, spin rotation and magnetic domain wall motion, as described in the formula below.

$$\mu' = 1 + x_{dw} = 1 + k \frac{M_s^2 D}{\delta \beta^{2/3}}$$
 (1)

Where x_{dw} is the magnetization of the domain wall motion, $M_{\rm S}$ is the saturation magnetization strength, D is the grain size, β is the impurity concentration, and δ is the thickness of the domain wall [11, 15]. As the BBSZ-LMZBS content increases, the grain size increases, resulting in a decrease in the number of grain boundaries per unit volume, thereby reducing the obstacles to domain wall movement. Although when the amount of BBSZ-LMZBS added is too large, the grains stick together, resulting in an increase in the average grain size, the addition of nonmagnetic BBSZ-LMZBS glass particles not only increases the impurity concentration, but also forms pinning points for the movement of magnetic domain walls, ultimately leading

to a decrease in initial magnetic permeability [16].

Fig. 5 shows the complex permittivity of NiCuZn between frequency of 1 MHz–1 GHz. Fig. 5a is a graph of the dielectric constant measured as a function of frequency, and Fig. 5b is a graph of the measured dielectric loss tangent ($\tan \delta$). The magnitude of the real (ε ') and imaginary (ε ") part of the dielectric constant of NiCuZn samples at room temperature are calculated using the formula:

$$\varepsilon' = C_p d / \varepsilon_0 A \tag{2}$$

and

$$\tan \delta = \varepsilon'' / \varepsilon' \tag{3}$$

Where C_p represents capacitance of the pellet, d is the pellet thickness, A is the surface area of the pellet, and ε_0 is the free space permittivity (8.854 \times 10⁻¹² F/m). The ε' and ε'' is stored energy and dissipated energy, respectively. The ratio $(\varepsilon''/\varepsilon')$ provides the tan δ . As the BBSZ-LMZBS content increased, for x=0.05 \sim 0.40, the values of ε' at 1 MHz were 21.8, 13.9, 13.8, 13.8, 13. 7, 13.8, 12.9, and 13.6, respectively. When the doping amount of BBSZ-LMZBS is $0.05 \le x \le 0.40$, the ε' maintains a stable value (13.9 – 12.9). When x=0.05, the ε' is 21.8, and then drops sharply to 13.9 (x=0.10). The doping of BBSZ-LMZBS can adjust the dielectric stability. When $0.0 \le x \le 0.40$, the dielectric properties of the samples remain stable in the frequency range of 1–100 MHz. The $tan\delta$ was small and ranged from 0.001~0.004. Due to the greater the dielectric loss of the device during operation, the more energy it consumes and the higher the temperature of the device, $tan\delta$ is an important evaluation parameter for electronic device materials [10]. The increase in temperature will further reduce the performance of the device and even cause irreversible damage to the device. The doping of BBSZ-LMZBS keeps $tan\delta$ at a lower value, promoting the application prospects of the material.

3.4. Gyromagnetic performance

Fig. 6 shows ferromagnetic resonance (FMR) line widths (ΔH) measured for the NiCuZn samples with various amounts

of added BBSZ-LMZBS and the corresponding fits to a Lorentz function. ΔH were measured at a frequency of 9.55 GHz, and the experimental data of samples were

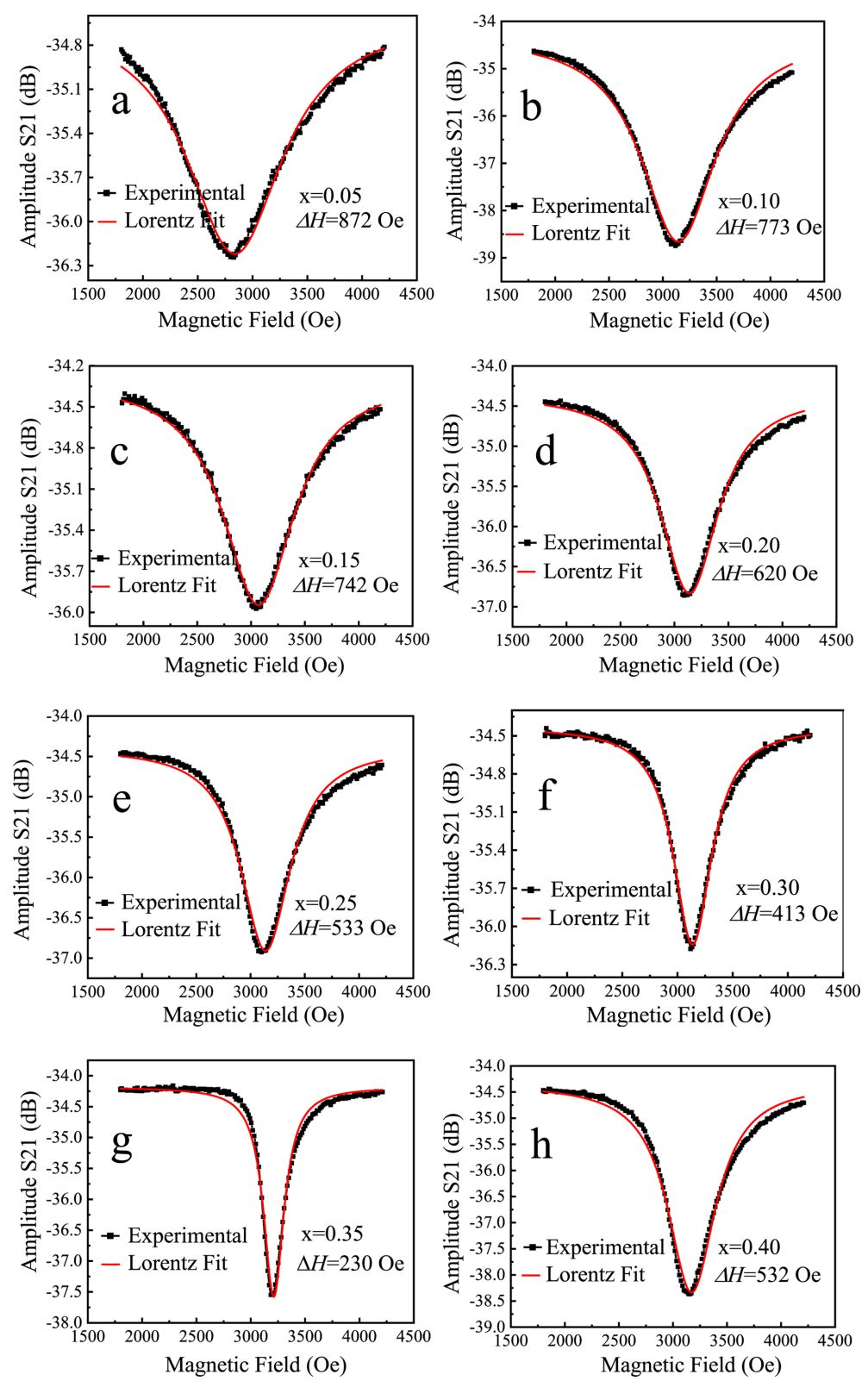


Fig. 6. (Color online) FMR line width of NiCuZn samples with different x contents of BBSZ-LMZBS.

-									
-	Sample	ST (°C)	M _s (emu/g)	H _c (Oe)	μ' (max)	ε' (min)	$\Delta H(\min)$	Ref.	
	NiCuZn	950	70.3	6.6	/	/	277	[18]	
	NiCuZn+BBSZ-LMZBS	880	94.42	81.84	30.6	12.9	230	This work	
	NiCuZn+BBSZ-Nb ₂ O ₅	880	32.61	28.6	212.2	21.4	280	[10]	
	NiCuZn+Bi ₂ O ₃ -MnO ₂	800	85.5	58.2	70.5	10.55	259	[19]	

Table 1. Comparison of main parameters between this work and other doped with Bi₂O₃ or BBSZ.

fitted with the Lorentz equation by the following formula 4,

$$y = y_0 + (2 \times A / \pi) \left\{ w / \left[4 \times (x - x_c)^2 + w^2 \right] \right\}$$
 (4)

This Lorentz fit better described the data when the ferromagnetic resonance line. For ferrite materials, ΔH is a key parameter of microwave devices. The ΔH consists of the intrinsic linewidth (ΔH_i) , the anisotropic linewidth (ΔH_a) , the porosity linewidth (ΔH_p) , the surface linewidth (ΔH_s) and the fast relaxation line width (ΔH_r) . Since the sphere has been finely polished during the test, the contribution of ΔH_s and ΔH_r is almost eliminated. The line width can also be expressed as:

$$\Delta H = \Delta H_i + \Delta H_a + \Delta H_p \tag{5}$$

 ΔH is mainly affected by ΔH_a and ΔH_p , and the ΔH_i is small and can be ignored. The ΔH_a comes from the anisotropic field fluctuation formed by the irregular distribution of magnetocrystalline anisotropic field in each grain. ΔH_p is mainly affected by the saturation magnetization M_s and the porosity P. The ΔH_p was approximately calculated by the following formula (6),

$$\Delta H_p = 1.5 \left(4\pi M_s \right) P \tag{6}$$

In this study, the ΔH with 0.05 to 0.40 calculated by Lorentz fit were 872 Oe, 773 Oe, 742 Oe, 620 Oe, 533 Oe, 413 Oe 230 Oe, and 532 Oe, respectively. With the increase of BBSZ doping amount, the ΔH shows a trend of first increasing and then decreasing. This is because when the BBSZ-LMZBS doping amount is small, the sample fails to sinter into a phase well. As BBSZ-LMZBS increases to 0.35, the crystal crystallization effect of the sample is better, its microstructure is further optimized, and the ferromagnetic resonance line width decreases. ΔH reaches a minimum value of 230 Oe at x=0.35. When BBSZ-LMZBS is further increased to x=0.40, the grain growth rate is faster than the densification rate, and some abnormal grains appear, which makes the uniformity of NiCuZn sample organization worse, and a small number of pores are formed, resulting in a gradual increase in ΔH [17]. The ΔH can be adjusted by controlling the doping amount of BBSZ-LMZBS.

In addition, Table 1 presents a comparison of the key parameters between this study and the reported ferrites doped with Bi_2O_3 or BBSZ. Similar to other reports, BBSZ-LMZBS doping in this study significantly reduced the ΔH value of NiCuZn sample. However, due to the imperfect microstructure caused by the synthesis process, the ΔH is still slightly large, which needs to be further improved in subsequent work.

4. Conclusions

A solid-phase preparation process was used to synthesize BBSZ-LMZBS doped Ni_{0.22}Cu_{0.31}Zn_{0.47}Fe₂O₄ samples, and the regulatory effect of different BBSZ-LMZBS contents on the microstructure as well as the static magnetic, soft magnetic and gyromagnetic properties of the sample were investigated and discussed in detail. With the increase of BBSZ-LMZBS doping amount, M_s and μ' show a trend of increasing first and then decreasing, H_c shows a trend of monotonically decreasing, and ΔH shows a trend of decreasing first and then increasing. As a new type of additive, BBSZ-LMZBS can significantly regulate the static magnetic, soft magnetic and gyromagnetic properties of NiCuZn, making the low-temperature sintered NiCuZn ferrite exhibit excellent magnetic properties. In summary, NiCuZn materials suitable for BBSZ-LMZBS co-doping have broad application prospects in the field of microwave communications devices.

References

- [1] H. Zhang, M. Du, J. Li, and L. Li, Ceram. Int. **50**, 34385 (2024).
- [2] A. Baykal, Y. Slimani, M. A. Almessiere, A. D. Korkmaz, H. Güngüneş, S. Caliskan, E. Arslan, and S. E. Shirsath, J. Mol. Struct. 1319, 139487 (2025).
- [3] X. Fan, G. Bai, Z. Zhang, Q. Chen, J. Jin, J. Xu, X. Zhang, and M. Yan, J. Adv. Ceram. 11, 912 (2022).
- [4] F. Xu, Y. Yang, X. Shi, Y. Liao, Y. Liu, X. Wang, F. Xie, and J. Hu, J. Alloys Compd. **885**, 160957 (2021).
- [5] X. Lu and L. Zhang, Micromachines. 15, 215 (2024).
- [6] B. B. Patil, J. Indian Chem. Soc. 100, 100811 (2023).
- [7] X. Wang, H. Zhang, L. Shi, J. Li, L. Jin, L. Cheng, L. Jia,

- D. Zhang, and Y. Liao, Ceram. Int. 48, 19011 (2022).
- [8] S. Wang, Y. Li, F. Li, M. Qu, Y. Liao, and Q. Wen, J. Magn. Magn. Mater. 576, 170773 (2023).
- [9] Y. Zhang, X. Tang, X. Wu, J. Chen, Y. Jing, and H. Su, J. Magn. Magn. Mater. 555, 169368 (2022).
- [10] Q. Li, J. Wang, and H. Yao, Ceram Int. 48, 8653 (2022).
- [11] Z. Cheng, X. Wang, X. Huo, Y. Jing, and H. Su, J. Magn. Magn. Mater. 603, 172256 (2024).
- [12] X. Huo, L. Xu, Y. Zhang, J. Liang, Y. Jing, and H. Su, J. Am. Ceram. Soc. 106, 7523 (2023).
- [13] H. Li, J. Wang, S. Lv, C. Chen, H. Luo, Q. Wu, Q. Zhang, H. Zheng, and L. Zheng, Ceram. Int. 50, 25925 (2024).

- [14] Y. Peng, C. Xia, M. Cui, Z. Yao, and X. Yi, Ultrason. Sonochem. **71**, 105369 (2021).
- [15] Z. Cao, Y. Jiang, Y. Tang, L. Wu, R. Luo, B. Wei, and T. Wang, J. Alloys Compd. 988, 174184 (2024).
- [16] B. Xia, D. Zhang, J. Li, Y. Li, and Y. Liao, J. Mater. Sci: Mater. Electron. 34, 2081 (2023).
- [17] Y. Yang, J. Li, H. Zhang, J. Li, F. Xu, G. Wang, F. Gao, and H. Su, Ceram. Int. 48, 12490 (2022).
- [18] H. Yang, Y. Ren, F. Xu, Y. Liao, X. Li, G. Liu, and B. Dai, J. Eur. Ceram. Soc. 45, 117484 (2025).
- [19] Q. Li, X. Zhang, G. Kou, and Y. Guo, J. Mater. Sci: Mater. Electron. 35, 1174 (2024).